PKA-dependent dynein switching from lysosomes to adenovirus: A novel form of host–virus competition

Julian Scherer, Julie Yi, and Richard B. Vallee

Department of Pathology and Cell Biology, Columbia University, New York, NY 10032

Cytoplasmic dynein is responsible for transport of several viruses to the nucleus. Adenovirus recruits dynein directly. Transport depends on virus-induced activation of protein kinase A (PKA) and other cellular protein kinases, whose roles in infection are poorly understood. We find that PKA phosphorylates cytoplasmic dynein at a novel site in light intermediate chain 1 (LIC1) that is essential for dynein binding to the hexon capsid subunit and for virus motility. Surprisingly, the same LIC1 modification induces a slow, but specific, dispersal of lysosomes (lyso)/late endosomes (LEs) that is mediated by inhibition of a newly identified LIC1 interaction with the RILP (Rab7-interacting lysosomal protein). These results identify an organelle-specific dynein regulatory modification that adenovirus uses for its own transport. PKA-mediated LIC1 phosphorylation causes only partial lyso/LE dispersal, suggesting a role for additional, parallel mechanisms for dynein recruitment to lyso/LEs. This arrangement provides a novel means to fine tune transport of these organelles in response to infection as well as to developmental and physiological cues.

Introduction

Subcellular transport and redistribution of diverse intracellular cargoes is controlled by microtubule (MT) motor proteins. Multiple mechanisms for recruitment of motors and for regulation of their mechanochemical activity have been described (Caviston and Holzbaur, 2006; Kardon and Vale, 2009; Vallee et al., 2012), but their relative importance in physiological cargo transport is incompletely understood. Pathogenic cargoes, especially viruses, also depend on the cellular transport machinery (Greber and Way, 2006; Radtke et al., 2006; Enquist, 2012). These agents have historically proven valuable in revealing and elucidating general cell biological concepts and have now become of interest as tools to understand mechanisms of motor regulation and recruitment as well (Dodding and Way, 2011; Scherer and Vallee, 2011).

This study was initiated to understand physiological mechanisms for regulation of cytoplasmic dynein cargo recruitment and activity. Dynein associates with diverse cellular structures, in each case using multiple cargo binding factors, including dynactin, NudE and NudEL, BicD2, and ZW10, alone or in combination (Kardon and Vale, 2009; Vallee et al., 2012). Some of the recruitment mechanisms also control motor output (King and Schroer, 2000; McKenney et al., 2010), but otherwise, the basis for the complexity in dynein recruitment factors remains poorly understood.

Ad5 (adenovirus serotype 5) has served experimentally as a relatively simple, well-defined, biochemically manipulable form of dynein cargo, which has already proven useful in efforts toward a more complete understanding of dynein recruitment and control (Bremner et al., 2009). Adenovirus enters the cell by receptor-mediated endocytosis (Chardonnet and Dales, 1970; Greber et al., 1993), during which the capsid subunit hexon is primed by the reduced pH endosomal environment for dynein binding (Bremner et al., 2009). Upon escape to the cytoplasm, the virus uses dynein to travel along MTs to the nucleus (Suomalainen et al., 1999; Leopold et al., 2000; Bremner et al., 2009). Interestingly, dynein binds via two of its cargo binding subunits, the intermediate chains (ICs) and light intermediate chain 1 (LIC1), directly to the adenovirus capsid (Bremner et al., 2009). This mechanism appears to be much simpler than that for physiological forms of cargo, though virus transport behavior is still regulated by dynactin (Bremner et al., 2009; Engelke et al., 2011).

Correspondence to Richard B. Vallee: rv2025@columbia.edu

J. Scherer's present address is Dept. of Molecular Biology and Princeton Neuroscience Institute, Princeton University, Princeton, NJ 08544.

Abbreviations used in this paper: IC, intermediate chain; LE, late endosome; LIC, light intermediate chain; MT, microtubule; NAGT, *N*-acetylglucosaminyltransferase I; p.i., postinfection; PKI, PKA inhibitor; PPase, phosphatase; RILP, Rab7-interacting lysosomal protein.

The Rockefeller University Press $30.00
J. Cell Biol. Vol. 205 No. 2 163–177
www.jcb.org/cgi/doi/10.1083/jcb.201307116

The current work addresses the role of protein kinases, especially PKA, in dynein-mediated transport processes. PKA, in particular, has been implicated in several of the few known mechanisms for modulating the motility of physiological cargo, though the underlying role of PKA is unknown (Reilein et al., 1998; Marks and Seabra, 2001; Rodionov et al., 2003). Host cell activation of PKA is also required for adenovirus transport, providing a potentially useful model system for understanding regulation of dynein cargo transport (Suomalainen et al., 2001).

We report that PKA phosphorylation of LIC1 is essential for dynein recruitment to the virus capsid and also for a decrease in dynein activity at lysosomes (lyso)/late endosomes (LEs). The latter effect is mediated by a loss of LIC1 from its lyso/LE receptor, which we identify as the Rab7-interacting lysosomal protein (RILP). These results identify a novel host cell response to virus infection and the first mechanism by which dynein-driven transport is tuned for controlled organelle redistribution. Finally, they suggest an evolutionary scenario through which this novel reciprocal virus–host behavior may have arisen.

Results

PKA effects on dynein–adenovirus interaction

Adenovirus represents a very well-defined form of dynein cargo, which can be readily manipulated and investigated in vivo and by use of biochemical approaches in vitro. We have been able to elucidate the mechanism for its dynein recruitment completely, which we found to involve interactions between the major capsid subunit hexon and the dynein ICs (IC1 and IC2) and LIC1, as expressed in mammalian cells (Bremner et al., 2009). Using bacterially expressed dynein subunits, we have since confirmed the IC–hexon interaction, but we found the LIC1 interaction to be very weak, suggesting a regulatory role for a LIC1 modification (unpublished data). In support of this possibility, we found that lambda phosphatase (PPase) treatment of purified rat brain dynein (Paschal et al., 1987) reduced its binding to hexon by 71 ± 17% (mean ± SD, $n = 3$; Fig. 1 A). To test a potential role for dynein phosphorylation in this interaction more directly, we subsequently exposed the dephosphorylated motor protein to purified PKA catalytic subunit plus ATP. This treatment more than reversed the effect of PPase treatment. We also exposed purified dynein to PKA phosphorylation alone, a treatment that enhanced hexon binding as well (Fig. 1 A).

To test which dynein subunits mediate these effects, the dynein complex was subjected to immunoblotting using an antibody to the phosphorylated PKA consensus sequence RRXp(S/T) (Fig. 1 B). The dynein ICs, as well as LIC1, each showed markedly enhanced PKA-dependent immunoreactivity, whereas other dynein subunits were negative (Fig. 1 B and not depicted). These results were confirmed by in vitro phosphorylation of individual bacterially expressed dynein subunits, which showed PKA-dependent phosphorylation of free IC1 and LIC1 but not of IC2, LIC2, LC8, TcTex-1, or Roadblock/LC7 (Fig. 1 C and not depicted).

To test the functional consequences of PKA phosphorylation, bacterially expressed dynein subunits were subjected to pull-down with hexon. LIC1–hexon binding was almost completely dependent on PKA phosphorylation, whereas IC binding showed no such requirement (Fig. 1 C). These results together suggest that LIC1 represents the dynein subunit, which confers sensitivity to PKA phosphorylation, although the ICs also likely contribute to dynein recruitment by adenovirus.

To identify the region within LIC1 responsible for this behavior, we tested overlapping mammalian cell-expressed fragments for hexon binding. The interaction site was localized within LIC1 residues 174–348 (unpublished data), which contains a single PKA consensus phosphorylation site (T213) conserved from frog to human and absent in LIC2. We found mutations in T213 (LIC1-T213A and -T213D) to abolish phosphorylation with recombinant PKA catalytic subunit (Fig. 1 D). Furthermore, LIC1-T213D, but not LIC1-T213A, bound hexon and competed with the dynein complex for hexon binding (Fig. 1 D and Fig. S1 A).

We used RNAi to elucidate the contribution of dynein LIC1 and LIC2 to cytoplasmic transport of adenovirus (Ad5, unless stated otherwise). Knockdown of LIC1 or LIC2 reduced protein levels at 48 h after transfection by 98 and 87%, respectively (Fig. 2 A). However, we found only small differences in virus infectivity using a standard assay measuring expression of GFP encoded in the viral genome (unpublished data). We reasoned that the prolonged test period might limit the sensitivity of the assay because residual virus particles remaining in the cytoplasm may still reach the nucleus through random movements and induce virus gene expression. To minimize such an effect, we modified the infectivity assay (see Materials and methods) by pretreating capsids with anti-hexon antibody. This treatment should activate a recently described cytoplasmic antiviral response (Mallery et al., 2010; McEwan et al., 2013) and lead to degradation of the lagging virus particles. We now observed clear reduction in infectivity, interestingly, in LIC1, but not LIC2, RNAi cells (Fig. 2, B and C).

At the cytological level, LIC1 RNAi also strongly inhibited virus redistribution to the nucleus to an extent similar to that from complete MT depolymerization using nocodazole (Fig. 2, D and E). Analysis of live virus motility also revealed a dramatic reduction in overall virus movement, which was reflected in a decrease in particle run length (Fig. 2 F and Fig. S2, Videos 1–3, and Table S1). Both directions of movement were affected, as is often observed from long-term dynein or kinesin inhibition (Kim et al., 2007; Ally et al., 2009; Bremner et al., 2009; Yi et al., 2011).

Because Ad5 infection induces PKA phosphorylation of LIC1 (Fig. S1 B), we tested the effects of LIC1 phosphorylation mutants in RNAi rescue experiments. Expression of RNAi-resistant versions of LIC1 wild type or the LIC1-T213D phosphomimetic mutant, but not LIC1-T213A or LIC2 wild type, rescued the effects on nuclear adenovirus redistribution induced by LIC1 knockdown (Fig. 3, A, B, and E). Rescue of directed virus motility was also observed by live imaging (Fig. S3, Videos 4–6, and Table S1), and virus run lengths were substantially restored, further supporting a role for PKA-mediated LIC1 phosphorylation in virus transport to the nucleus (Fig. 3 C). Interestingly, adenovirus redistribution was inhibited by LIC1 RNAi to an extent comparable to that achieved using the PKA inhibitors

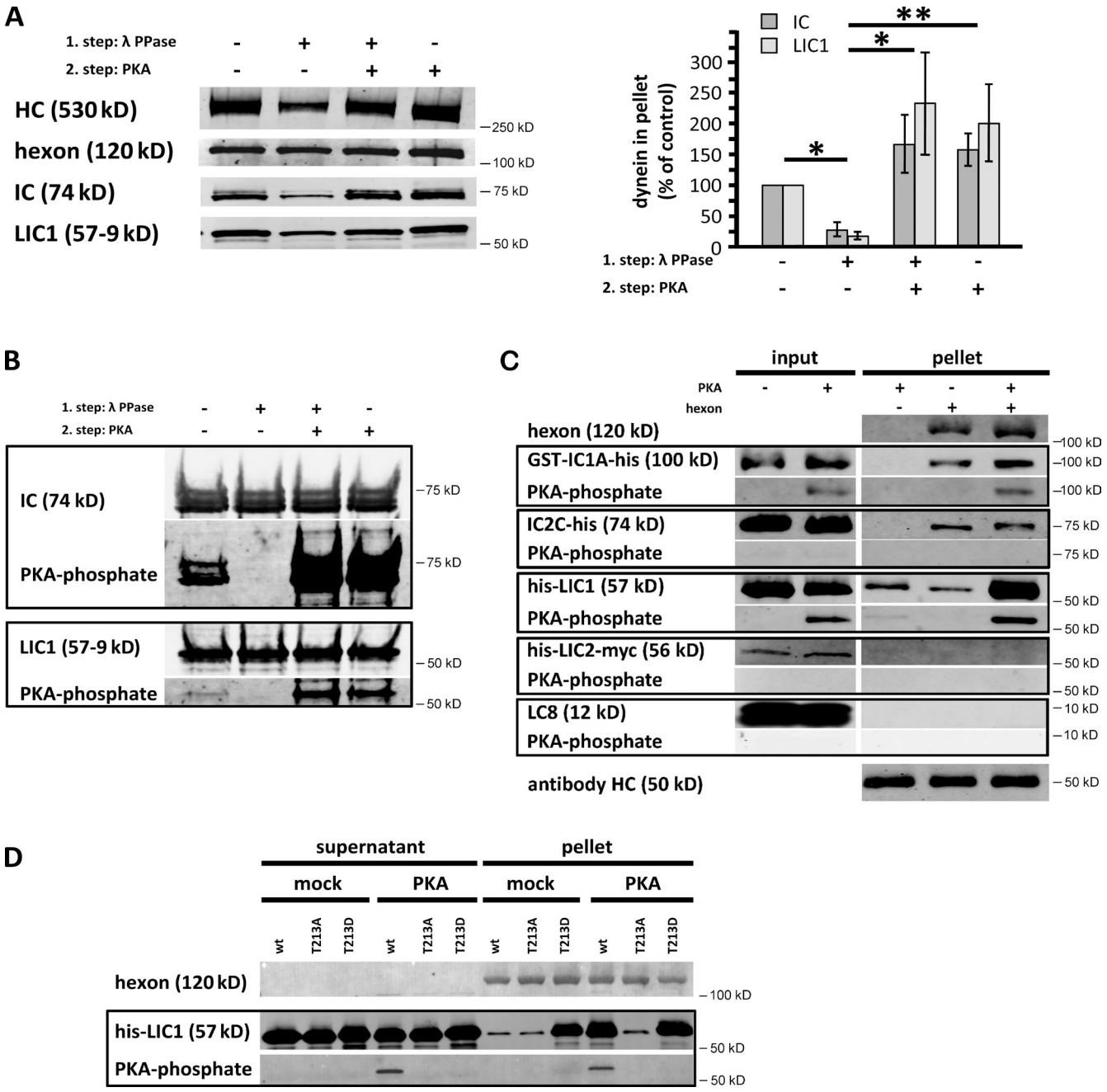

Figure 1. **PKA phosphorylation of the dynein LIC1 subunit controls binding to adenovirus hexon subunit.** (A) Purified rat brain cytoplasmic dynein was exposed to λ-phosphatase (PPase) and/or protein kinase A (PKA) catalytic subunit and evaluated for coimmunoprecipitation with hexon by immunoblotting of the pellets with antibodies against hexon, and dynein heavy chain (HC), intermediate chain (IC), and light intermediate chain (LIC) subunits. (right) Quantification of IC and LIC1 immunoblotting results: $n = 3$, mean ± SD, mock treated = 100%. Dynein dephosphorylation decreased and PKA treatment enhanced binding to hexon. *, $P < 0.05$; **, $P < 0.01$ (based on LIC1 signal). (B) Pretreated dynein was evaluated by immunoblotting with antibodies against the dynein ICs, LIC1, and the phosphorylated PKA consensus sequence RRXp(S/T). Clear phosphorylation of the IC and LIC1 subunits is observed. (C) Bacterially expressed full-length dynein subunits IC1, IC2, LIC1, LIC2, and LC8 were exposed to PKA catalytic subunit and tested for phosphorylation and hexon coimmunoprecipitation by immunoblotting with the anti-RRXp(S/T) antibody. LIC1 and IC1 were clearly phosphorylated, which specifically increased LIC1 binding to the hexon. (D) Bacterially expressed LIC1 wild type or the LIC1-T213A and -T213D mutants were tested for PKA phosphorylation and hexon coimmunoprecipitation. The phosphomimetic LIC1-T213D mutant alone interacted with hexon. No PKA phosphorylation was detected in the mutant polypeptides, identifying T213 as the major PKA site. wt, wild type.

(PKIs) PKI-myr (myristoylated) or H-89 (Fig. 3, D and E; and not depicted), suggesting that PKA phosphorylated LIC1 plays a substantial role in controlling adenovirus transport.

As an additional test for the role of LIC1 phosphorylation in virus transport, we combined RNAi rescue with PKA inhibition. As expected, untransfected controls and knockdown cells rescued with LIC1 wild type remained sensitive to PKA inhibition as indicated by impaired nuclear targeting of adenovirus (Fig. 3, D and E). Cells rescued with LIC1-T213D became much less sensitive to PKA inhibition (Fig. 3, D and E),

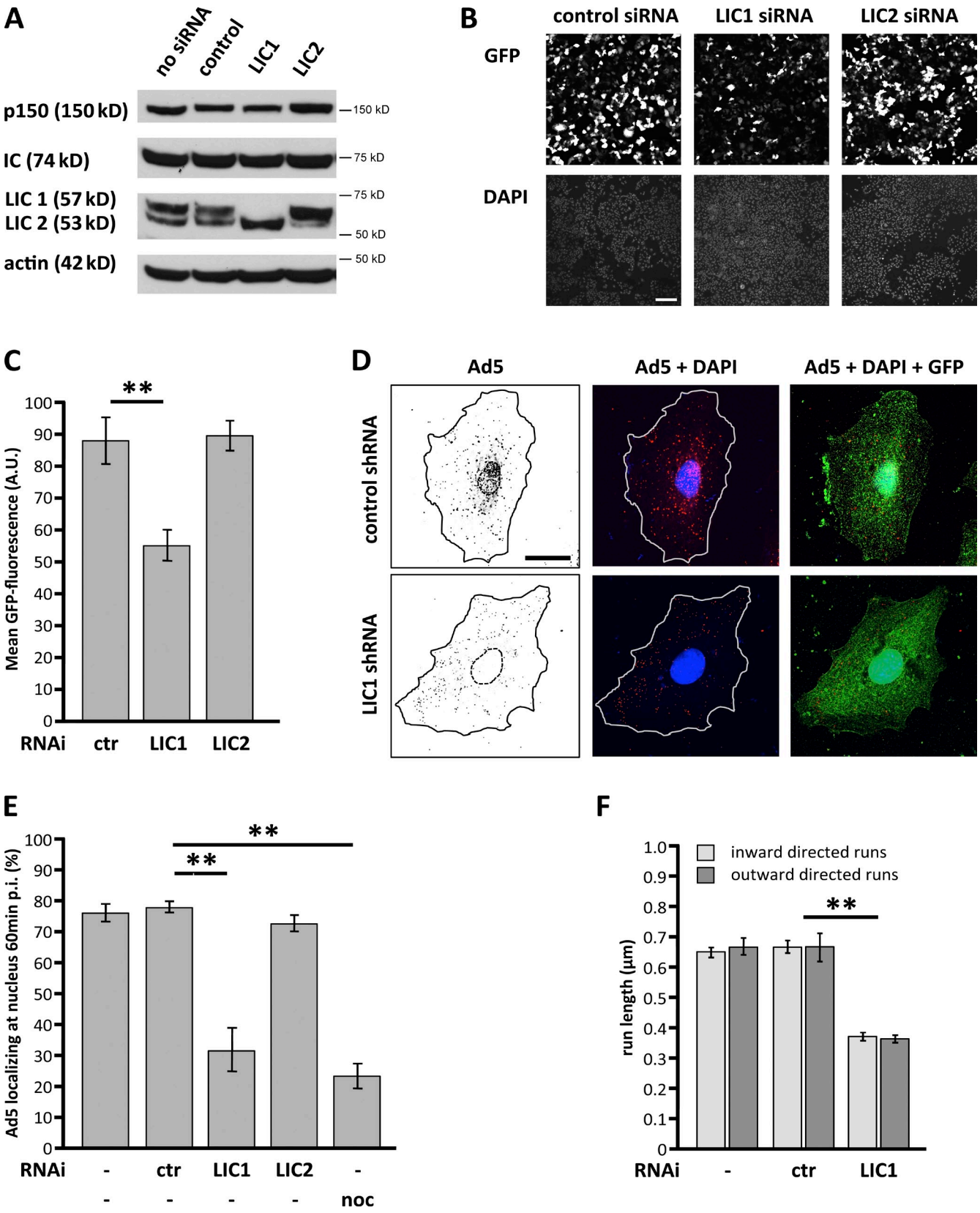

Figure 2. **Effects of LIC RNAi on Ad5 transport.** (A) Protein levels in lysates of A549 cells transfected with control, LIC1-, or LIC2-targeted siRNAs for 48 h evaluated by immunoblotting using anti-p150^{Glued}, anti-IC, and anti–pan-LIC antibodies, with anti-actin as a loading control. LIC1 was reduced by 98%, and LIC2 was reduced by 87%. (Note that moderate increase of LIC2 levels in LIC1 knockdown lane, and vice versa, suggests possible compensatory up-regulation.) (B) LIC RNAi effect on adenovirus infectivity. Ad5-GFP infectivity was examined in A549 cells transfected with LIC1, LIC2, or control siRNAs 48 h before infection with antibody-labeled Ad5 (see Materials and methods). At 24 h p.i., fixed cells were counterstained for DNA (DAPI). LIC1 siRNA inhibited Ad5 infectivity, an effect not detected for control or LIC2 siRNA. Bar, 200 µm. (C) Quantification of virus infectivity shown in B. Mean GFP fluorescence

though a small residual degree of inhibition raises the possibility of a potential role for additional PKA substrates in capsid redistribution.

Host organelle behavior

These results provide the first detailed insight into a host cell signaling mechanism responsible for controlling motor protein-mediated virus transport. Presumably, however, this mechanism emerged not to aid in virus infection but for host cell protection and might, therefore, have a role in some form of dynein-mediated host defense against adenovirus. To explore this possibility, we evaluated the effect of Ad5 infection on host cell behavior. Cell morphology remained largely unchanged for up to 120 min post-infection (p.i.) with no obvious effect on MT and centrosome distribution (unpublished data). Because LICs have a specific role in controlling lyso/LE distribution (Tan et al., 2011), we monitored the behavior of these organelles by live microscopy of LysoTracker green–stained A549 cells for 90 min after Ad5 infection. Over this time period, lyso/LEs gradually dispersed from their usual perinuclear location to invade the more peripheral areas of the cytoplasm. Partial redistribution was detected within 15–30 min p.i., and complete dispersal occurred at 60 min (Fig. 4, A and B; Fig. S4; Videos 7, 8, and 10; and Table 1). Of note, the onset of lyso/LE dispersal correlates with the adenovirus-induced stimulation of PKA activity (15–30 min p.i.; Suomalainen et al., 2001) and endosomal escape of the capsids (∼15 min p.i.; Greber et al., 1993). Live imaging revealed a slow, but highly reproducible (39/46 cells; Table 1), spread of lyso/LEs particles. The clearest change could be observed in the initially empty peripheral region of the cell, whereas the perinuclear lyso/LE cluster became less prominent in most cells, as expected for partial dynein inhibition. These effects were much weaker than those we observed after severe, acute dynein inhibition (Yi et al., 2011). In the latter case, some cells showed detectable depletion of lyso/LEs from the cell center, which was not observed in adenovirus-infected cells, again suggesting less potent dynein inhibition. Bidirectional movement of individual lyso/LE particles could also be seen to persist throughout the virus-induced lyso/LE dispersal process. These results are together consistent with only partial inhibition of motor activity. This conclusion is supported by analysis of flux and run length for lyso/LE transport in virus-infected cells, which showed changes that were below the level of significance for both outward- and inward-directed movement (unpublished data). These results, we note, are entirely consistent with an ∼10-fold longer half-time for the virus-induced lyso/LE dispersal than that observed in acute dynein-inhibited cells (Yi et al., 2011).

Vesicular organelles positive for GFP-Rab7 and GFP-NPC1, a lyso/LE component implicated in cell entry by Ebola virus (Carette et al., 2011; Côté et al., 2011), also spread more broadly throughout the cytoplasm in response to Ad5 infection, similar to LysoTracker-positive vesicles (Fig. 4 C and Table 1). In contrast, markers for Golgi elements (*N*-acetylglucosaminyltransferase I [NAGT]–GFP) and mitochondria (MitoTracker), which change their motility and morphology during herpes virus infection (Kramer and Enquist, 2012), showed no obvious evidence of redistribution (Fig. 4 C and Table 1). These data are consistent with LysoTracker localization to organelles positive for GFP-Lamp1, -NPC1, -Rab7, and -RILP but not for GFP-Rab5 or -NAGT (Fig. S5) and indicate a specific dispersal of lyso/LE during Ad5 infection.

To test the role of PKA in virus-induced lyso/LE dispersal, we again inhibited the protein kinase itself using H-89 or upstream integrin signaling-induced cAMP production using a cyclic RGD peptide (Wickham et al., 1993; Suomalainen et al., 2001). Each condition caused pronounced inhibition of lyso/LE dispersal in virus-infected cells (Fig. 4 A, Video 9, and Table 1). Conversely, activation of adenylate cyclase using 10 µM forskolin also led to dispersal of lyso/LEs, phenocopying the effects of adenovirus infection (Fig. 4 A and Table 1) and suggesting that PKA activation is sufficient for dispersal. In addition, we used SB203580 to inhibit p38/MAPK, which is also activated during Ad5 challenge (Suomalainen et al., 2001), but we saw no effect on lyso/LE distribution (Fig. 4 A and Table 1).

To test whether the effects we observed on lyso/LE behavior occur in response to infection with other adenoviruses, we monitored lyso/LE distribution in cells infected with Ad3 (adenovirus 3). Ad3 is a species B adenovirus, which can activate PKA though integrins, like Ad5 (species C). However, in contrast to species C, species B adenoviruses are largely retained in the endolysosomal pathway for several hours (Miyazawa et al., 2001). We found Ad3 to induce clear PKA-dependent lyso/LE dispersal with similar kinetics to those for Ad5 (Table 1 and not depicted). Together, these data reveal that PKA-mediated lyso/LE dispersal is not unique to Ad5.

To test for a specific role of LIC1-T213 phosphorylation in lyso/LE dispersal, we again used LIC RNAi. LIC1 and LIC2 RNAi each disrupted lyso/LE organization (Tan et al., 2011), with clear dispersal observed in the A549 cells used in the current experiments (Fig. 5, A–C). Expression of RNAi-insensitive wild-type LIC1 prevented lyso/LE dispersal (Tan et al., 2011), as did LIC1-T213A, though LIC1-T213D had a significantly weaker effect (Fig. 5, A–C). Furthermore, LIC1-T213A rescue strongly inhibited lyso/LE dispersal in adenovirus-infected

per field of view at 24 h p.i. ± SD from three independent experiments. (D) LIC RNAi effect on adenovirus redistribution. A549 cells expressing LIC1 or control shRNA for 48 h were infected with Ad5 and fixed at 60 min p.i. Cells were immunostained for Ad5 and GFP and counterstained for DNA (DAPI). Adenovirus normally redistributes to the nucleus (control) but remains in the cell periphery in LIC1 RNAi cells. Lines define cell outlines. Bar, 20 µm. (E) Quantification of virus redistribution shown in D. Mean percentage of Ad5 particles localizing at the nucleus 60 min p.i. ± SD from three independent experiments with >30 cells each. LIC1 shRNA inhibited Ad5 redistribution similar to 10 µM nocodazole treatment, an effect not detected for control or LIC2 shRNA. (F) LIC1 RNAi effect on virus run length. A549 cells treated with LIC1 or control siRNA or mock treated were infected with Alexa Fluor 546–labeled Ad5 48 h later and imaged for particle tracking (see Materials and methods). LIC1 siRNA showed a significant reduction in virus run length. Error bars show SDs. **, $P < 0.01$. A.U., arbitrary unit; ctr, control; noc, nocodazole.

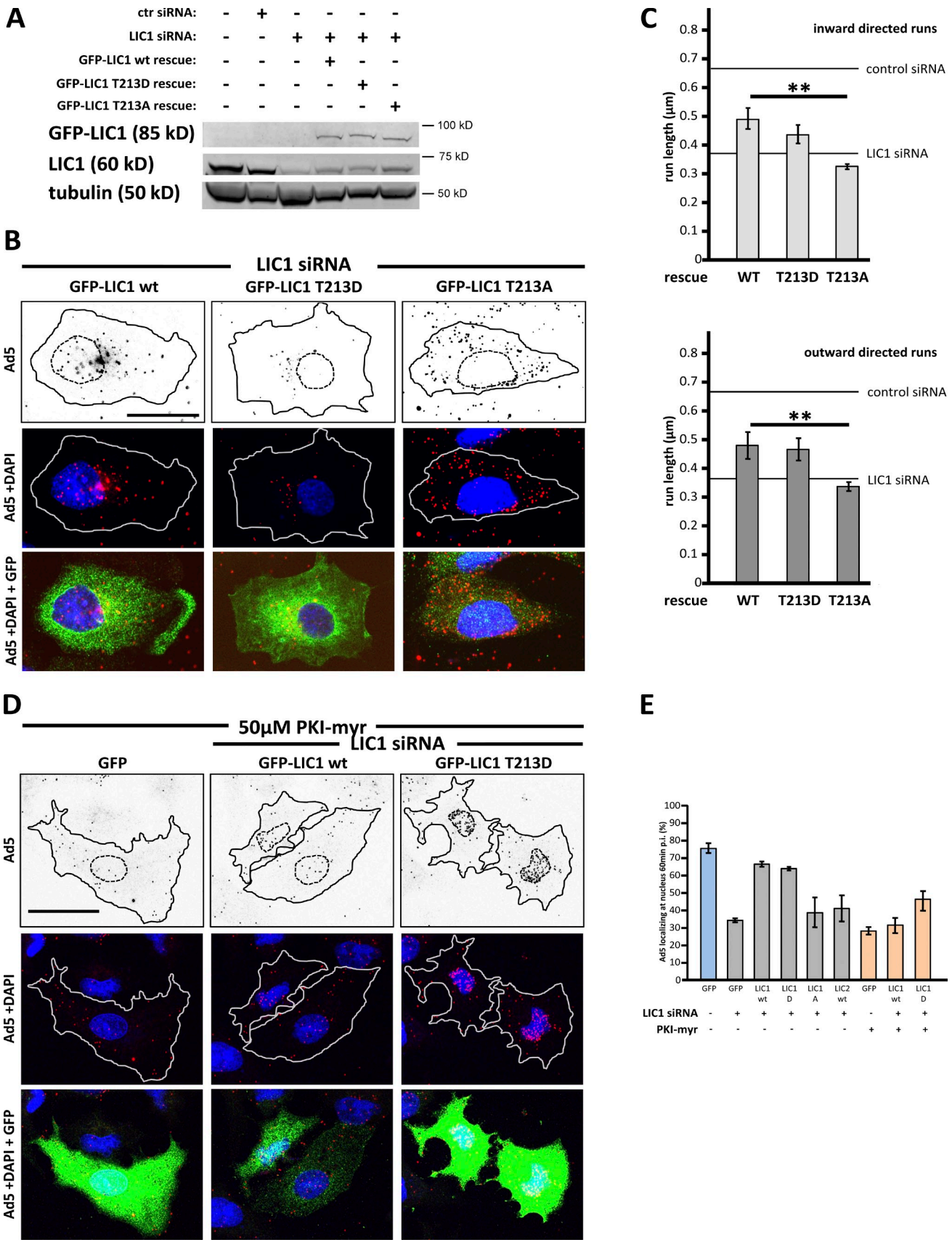

Figure 3. **Phosphorylated LIC1 is required for transport of adenovirus to the nucleus.** (A) Protein levels in lysates of A549 cells exposed to siRNAs (48 h) and expression of RNAi-resistant GFP-LIC1 (24 h) evaluated by immunoblotting using anti-LIC1 and anti-GFP antibodies, with anti-tubulin as a loading control. (B) LIC1 RNAi rescue of adenovirus redistribution. LIC1 siRNA-treated A549 cells transfected at 24 h with GFP-tagged LIC1 cDNAs (indicated on

cells, whereas LIC1 wild-type rescue showed no apparent effect (Fig. 5, D and E).

The nature of LIC binding to lyso/LEs was unknown. The dynein regulatory factor dynactin associates with these organelles via spectrin (Holleran et al., 1996) or via an interaction of the dynactin subunit p150^{Glued} with the N-terminal region of RILP (Jordens et al., 2001; van der Kant et al., 2013). RILP is itself recruited to lyso/LEs through an interaction with activated Rab7 (Cantalupo et al., 2001) and has a central role in lyso/LE positioning (Cantalupo et al., 2001; Progida et al., 2007; Rocha et al., 2009; Tan et al., 2011). We tested for a dynactin-independent interaction between the dynein LIC subunits and RILP. We observed clear coimmunoprecipitation with LIC1 and of LIC2, each coexpressed with full-length RILP in cultured mammalian cells (Fig. 6, A and B; and Fig. S1 C). The dynactin subunit p150^{Glued} was undetectable in LIC1 immunoprecipitates (Fig. S1 D), suggesting that it was not required for the LIC–RILP interaction. We found, in addition, that bacterially expressed LIC1 pulls down full-length or an N-terminal RILP fragment (RILP-C185) expressed in mammalian cultured cells (Fig. 6 C). The C-terminal RILP fragment (RILP-N217), in contrast, showed no detectable interaction with LIC1 (Fig. 6 C). In similar experiments, bacterially expressed RILP-C185 preferentially pulled down LIC1-T213A compared with LIC1 wild-type or LIC1-T213D expressed in mammalian cultured cells (Fig. 6, D and E), supporting a role for RILP in PKA-mediated dissociation of dynein from lyso/LEs. Finally, we observed clear pull-down of purified rat brain dynein and of bacterially expressed LIC1 with the RILP-C185 fragment (Fig. 6 F and Fig. S1 E), further supporting a direct RILP–dynein interaction mediated by the LICs.

Discussion

Diverse factors have been implicated in dynein regulation, but little is known as to how, when, and to what purpose they are activated in the cell (Kardon and Vale, 2009; Vallee et al., 2012). In addition to advances made in the study of physiological cargoes, viruses are proving useful as model cargoes, which can be completely defined at the molecular level (Dodding and Way, 2011; Scherer and Vallee, 2011). We previously found adenovirus to recruit cytoplasmic dynein, but not dynactin, to the hexon capsid subunit after low pH priming (Bremner et al., 2009), providing insight into how virus transport is initiated after endosome escape. We now show evidence that this mechanism is further specifically activated by PKA. Our analysis has also provided insight into the less tractable problem of physiological cargo regulation, as it led us to discover clear PKA-mediated, LIC1-dependent redistribution of lyso/LEs to the cell periphery. The physiological importance of this phenomenon, its role in what we refer to as dynein "tuning," and the role for RILP in this process are discussed further in this section.

The targets for PKA phosphorylation in Ad5-infected cells have remained undefined (Suomalainen et al., 2001). We find that PKA phosphorylation enhances dynein binding to hexon and identified candidate PKA sites in IC1 and LIC1. However, PKA phosphorylation of LIC1 alone is sufficient to affect hexon binding and virus transport. RNAi against LIC1, but not LIC2, strongly reduces infectivity and nuclear targeting of adenovirus. We also detect significantly reduced virus motility in LIC1 RNAi cells, indicative of disrupted MT-based transport. We can rescue virus transport by overexpression of LIC1 wild type and the PKA phosphomimetic LIC1-T213D mutant but not the dephosphomutant LIC1-T213A or the non-PKA–phosphorylatable LIC2 wild type. These results provide strong additional evidence that LIC1-T213 is a crucial site and that its phosphorylation likely enhances virus transport by stimulating dynein recruitment to adenovirus. A role for additional PKA targets in adenovirus transport is possible, but the LIC1 PKA site appears to be largely, if not entirely, responsible.

The role of ICs in the dynein–Ad5 interaction is less clear. Recombinant LIC1 was sufficient to compete with the intact dynein complex for hexon binding, whereas comparable experiments using IC were negative (unpublished data). The ICs, therefore, may play a secondary role in dynein recruitment to adenovirus. The IC1 PKA site may, conceivably, have a role in interactions with its own physiological binding partners, a possibility suggested by the location of the sole PKA site (IC1-T59) within the dynactin and NudE/EL interaction region (McKenney et al., 2011; Barbar, 2012).

We found that PKA-mediated LIC1 phosphorylation affected only a single organelle class, lyso/LEs. Although LICs participate in a range of dynein functions, we have found these subunits to contribute to the motility of lyso/LEs but not other dynein-controlled vesicular organelles such as the Golgi apparatus (Tan et al., 2011), though a specific LIC1 function in Golgi integrity has been reported in one other study (Palmer et al., 2009). LIC1 phosphorylation appears from the current study to influence lyso/LE behavior by a specific reduction in dynein function. Lyso/LEs normally undergo short bidirectional movements in nonneuronal cells, driven by the opposing activities of dynein and kinesin (Herman and Albertini, 1983; Kim et al., 2007; Soppina et al., 2009; Caviston et al., 2011; Yi et al., 2011). Acute dynein inhibition unmasks outward movements and causes them to predominate, resulting in rapid lyso/LE dispersal (Yi et al., 2011). Adenovirus-induced lyso/LE dispersal might, in principle, result from dynein inhibition, kinesin activation, or both.

top) and infected at 48 h with Ad5 for 60 min. Cells were stained for Ad5, GFP, and DNA (DAPI). Transfected cells are outlined. LIC1 RNAi–inhibited redistribution is rescued by GFP-LIC1 wild type (wt) and GFP-T213D but not GFP-T213A. (Capsids outside the encircled cells are located in adjacent cells.) (C) LIC1 RNAi rescue effect on virus run length. A549 cells treated with LIC1 siRNA were subsequently transfected with LIC1 wild type, -T213D, or -T213A and infected with Alexa Fluor 546–labeled Ad5 48 h later and imaged for particle tracking (see Materials and methods). LIC1 wild type and phosphomimetic T213D mutant showed rescue in virus run length, in contrast to the LIC1 dephosphomutant T213A. Error bars show SDs. (D) LIC1 RNAi rescue of adenovirus redistribution like in B, in the presence of PKA inhibitor PKI-myr. The inhibitor alone (GFP) inhibited virus accumulation at the nucleus, whereas partial inhibition was observed in the RNAi rescue cells. Lines define cell outlines. (E) Quantification of virus redistribution shown in B and D. Mean percentage of Ad5 particles localizing at the nucleus 60 min p.i. ± SD from at least three independent experiments with >40 cells each. Blue, control condition; gray, summary of experiments for B; orange, summary of experiments for D. **, $P < 0.01$. ctr, control. Bars, 20 µm.

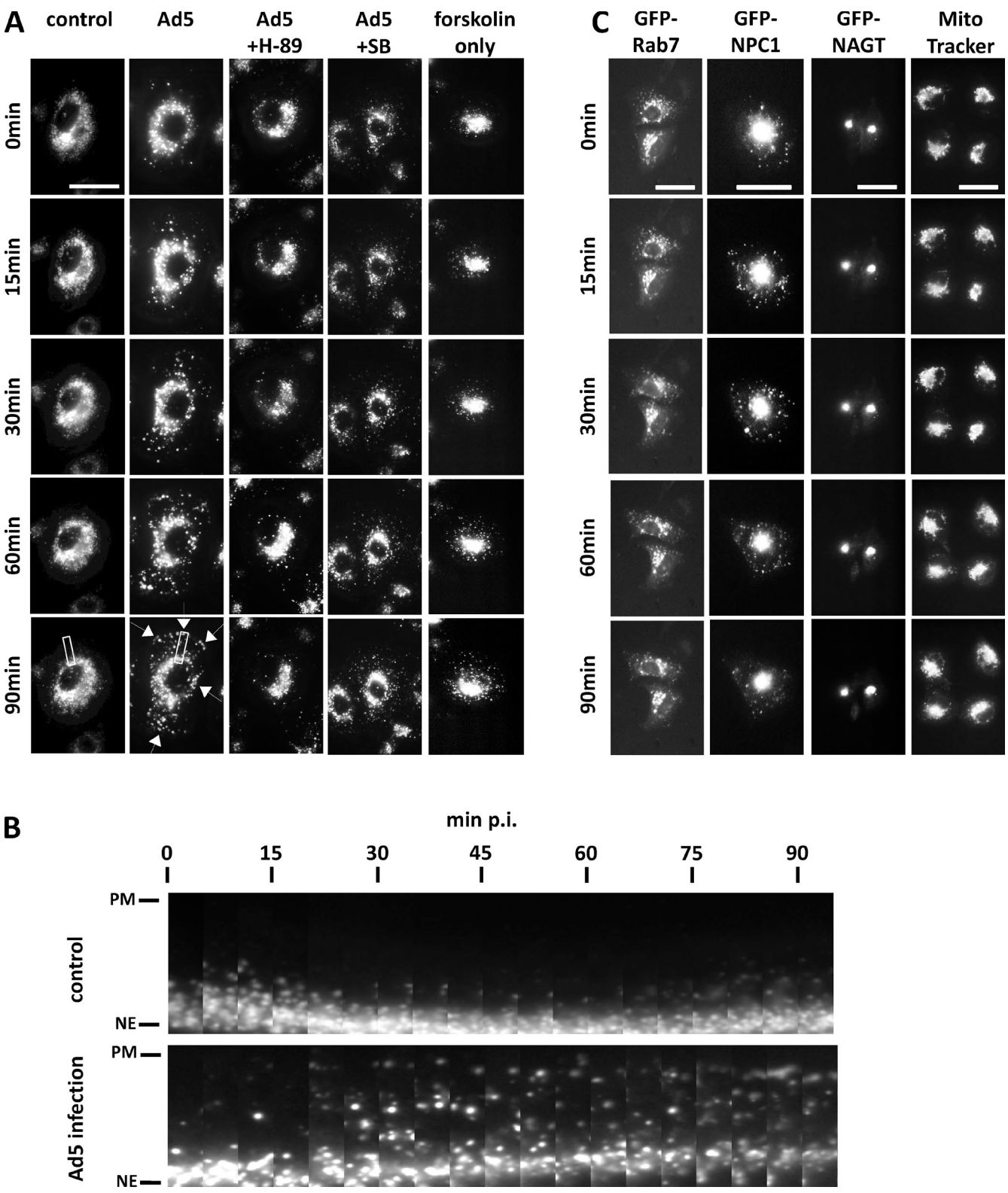

Figure 4. **Adenovirus infection induces specific lysosomal spread to the cell periphery in a PKA-dependent manner.** (A) Still images of 90-min videos of LysoTracker-stained A549 cells. Controls showed an unchanging perinuclear distribution of lyso/LEs. Ad5 infection caused dramatic lyso/LE dispersal, especially notable in the appearance of individual vesicles toward the cell periphery (arrowheads). This effect was inhibited by the PKA inhibitor H-89 (5 µM) but not by p38/MAPK inhibitor SB203580 (SB; 10 µM). Treatment of uninfected cells with the adenylyl cyclase activator forskolin (10 µM) caused lyso/LE dispersal with similar kinetics to those seen upon virus infection. Bar, 20 µm. (B) Series of enlarged images of boxed areas in A of control and Ad5 videos spanning from the nuclear envelope (NE) to the plasma membrane (PM). Frames were taken every 5 min. (C) Still images of 90-min videos of A549 cells expressing GFP-tagged vesicular markers for lyso/LEs (GFP-Rab7; GFP-NPC1), Golgi elements (GFP-NAGT), and mitochondria (MitoTracker green). Ad5 infection caused dispersal of Rab7- and NPC1-positive late endosomal vesicles, with no apparent effect on Golgi elements (*N*-acetylglucosaminyltransferase I [NAGT]) or mitochondria. Bars, 15 µm.

Table 1. **Effect of adenoviruses and PKA-targeting drugs on the dispersal of membranous organelles**

Organelle marker	Virus	Drug	Number of cells	Number of cells showing organelle dispersal	Cells showing organelle dispersal
					%
LysoTracker	–	–	31	5	16.1
LysoTracker	Ad5	–	46	39	84.8
LysoTracker	Ad5	H-89 (5 µM)	31	11	35.5
LysoTracker	Ad5	SB203580 (10 µM)	20	16	80.0
LysoTracker	Ad5	Cyclic RGD (8.5 µM)	15	6	40.0
LysoTracker	–	Forskolin (10 µM)	32	25	78.1
LysoTracker	Ad3	–	57	41	71.9
LysoTracker	Ad3	H-89 (5 µM)	32	5	15.6
GFP-Rab7	Ad5	–	18	12	66.7
GFP-Rab7	–	–	7	1	14.3
GFP-NPC1	Ad5	–	6	5	83.3
GFP-NPC1	–	–	4	0	0.0
GFP-NAGT	Ad5	–	13	0	0.0
GFP-NAGT	–	–	5	0	0.0
MitoTracker	Ad5	–	20	1	5.0
MitoTracker	–	–	4	0	0.0

Dispersal was scored based on 90-min time-lapse videos. Minus signs indicate that either no virus or no drug was added.

However, the failure of adenovirus to induce lyso/LE dispersal in LIC knockdown cells rescued with LIC1-T213A supports a prominent, specific role for cytoplasmic dynein. In further support of this hypothesis, we found LIC1 to interact directly with RILP, an interaction that appears to depend on LIC1-T213 phosphorylation.

Although the effect of PKA phosphorylation on lyso/LE behavior is very clear and reproducible, inhibition seems to be partial. This judgment is based on comparison of live lyso/LE behavior in the current study with the effects of acute dynein inhibition by injection of function-blocking antibodies or dominant-negative polypeptide fragments (Yi et al., 2011). In that case, lyso/LEs dispersed from the cell center to the periphery within 5–10 min, and in some cells, nearly complete depletion of lyso/LEs from the cell center was observed. How the cell could achieve specific, but only partial, dynein inhibition in the current study is uncertain. We suggest that this might be a reflection of redundant mechanisms (Vallee et al., 2012) for controlling dynein recruitment to lyso/LEs. We find that LIC2, which is not phosphorylated by PKA, binds RILP, suggesting a distinct LIC2-containing subpopulation of lyso/LE-associated dynein (Tan et al., 2011; Hunt et al., 2013), which is not under PKA control. Additional dynein recruitment factors, including NudE, NudEL, spectrin, ZW10, and dynactin have also been implicated in lyso/LE motility (Tan et al., 2011; Vallee et al., 2012). Their relative contributions to dynein recruitment remains to be determined, but our results provide the first suggestion that some of them remain active when the LIC1–RILP interaction is blocked. Such a mechanism should provide a finer level of motor tuning than would be achieved by complete dynein inhibition or complete loss of dynein from lyso/LEs. We note that most organelles may make use of multiple dynein recruitment factors (Akhmanova and Hammer, 2010; Vallee et al., 2012), raising the possibility that mechanisms for fine tuning minus-end transport may be a general phenomenon.

Our results suggest that the RILP–LIC interaction is direct and independent of $p150^{Glued}$, which has been reported to bind within the same N-terminal half of the RILP polypeptide (van der Kant et al., 2013). A similar arrangement has recently been reported for BicD2, which is recruited to Golgi membranes through C-terminal binding to activated Rab6 (Matanis et al., 2002) and forms a co-complex through its coiled-coil α-helical N-terminal region with dynein and dynactin. $p150^{Glued}$, dynein heavy chain, and LIC1 were each implicated in the BicD2 interaction by cross-linking analysis (Splinter et al., 2012). FIP3, which links dynein LICs to the recycling endosomal adapter Rab11, may be another example (Horgan et al., 2010). We propose, therefore, a new structural and functional grouping—the RDD (Rab–dynein–dynactin interacting) proteins—connecting vesicle-associated Rabs to both dynein and dynactin.

Our results reveal a remarkable use of a highly specific phosphorylation mechanism, involving a single PKA site within a unique LIC isoform, for opposite purposes by host and pathogen (Fig. 7). We speculate that the lyso/LE dispersal phenotype described here may increase the ability of degradative organelles to reach incoming viruses before they exit the endocytic pathway, perhaps to increase the chance of virus neutralization. In support of this possibility, Ad5 trapped in the endolysosomal compartment shows decreased infectivity (Carey et al., 2007). Intriguingly, *Trypanosoma cruzi* infection also induces lysosome redistribution to the cell periphery. In this case, however, lysosome fusion with the parasitophorous vacuole stimulates escape of the pathogen from the vacuole and enhances infection (Tardieux et al., 1992; Andrews, 1995). These observations raise the possibility that Ad5 might similarly take advantage of peripheral lyso/LEs to increase infectivity by inducing more rapid acidification of the uptake compartment and facilitating escape into the cytoplasm.

Our results suggest that, remarkably, adenovirus has evolved to make its own use of an underlying phosphorylation

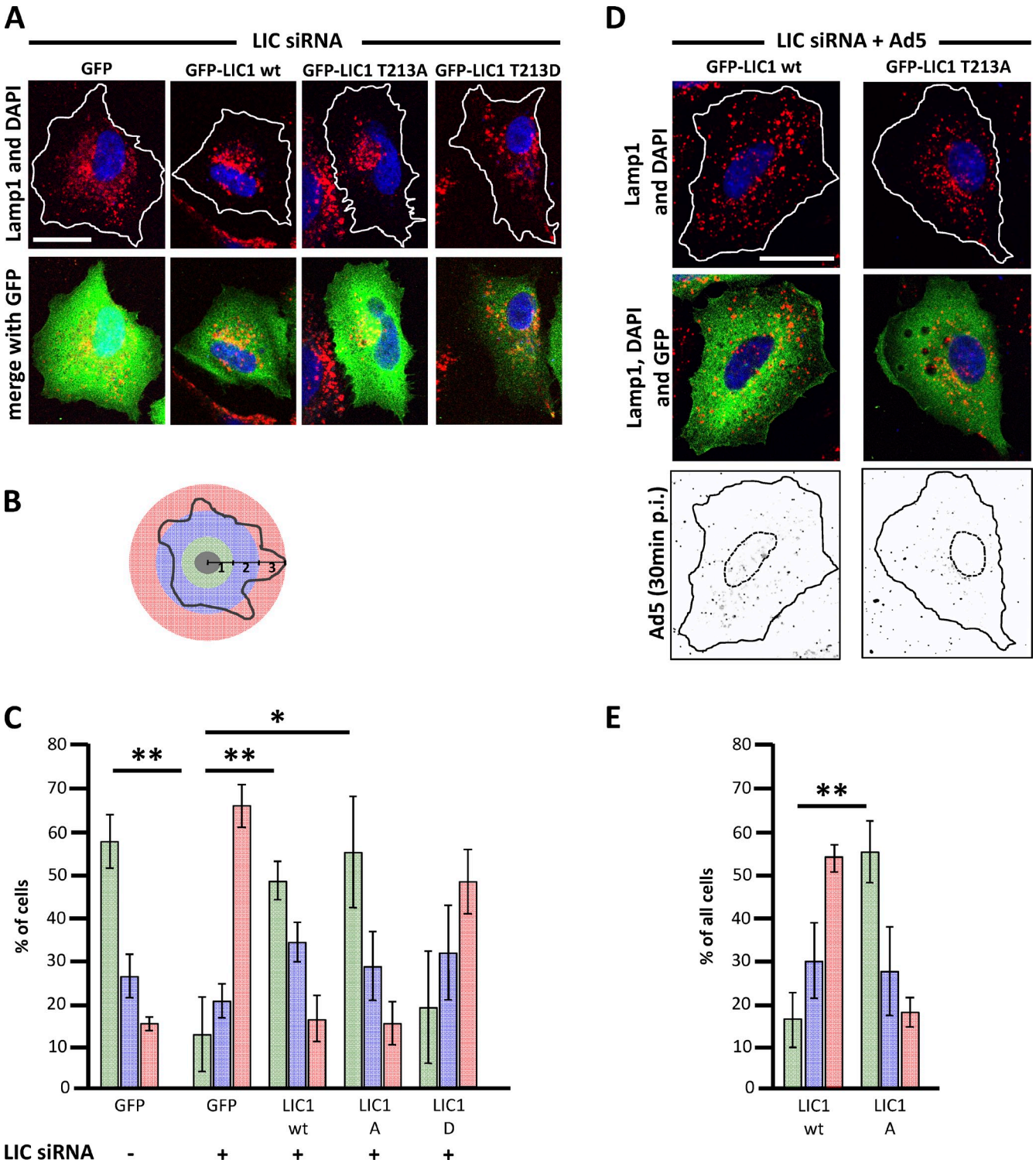

Figure 5. **Role of LIC1-T213 in lysosome dispersal.** (A) Rescue of LIC1/LIC2 RNAi-induced lyso/LE dispersal by overexpression of GFP (control), GFP-LIC1 wild type (wt), -T213A, or -T213D in A549 cells shown by immunostaining for GFP (green) and LAMP1 (red). Rescue was observed with GFP-LIC1 wild type and LIC1-T213A but not with LIC1-T213D or GFP. (B) Schematic representation of scoring procedure for lyso/LE dispersal. Cells are scored as strongly dispersed (red), if lysosomes can be detected within the outer, middle, and inner bands. They are scored as partially dispersed (blue) or normal (green) if lysosome localization does not extend beyond to the middle or inner bands, respectively. (C) Quantification of data in A. Mean of three independent experiments with >40 cells each; error bars represent SDs. (D) Role of LIC1-T213 in Ad5-induced lyso/LE dispersal. LIC RNAi rescue with LIC1-T213A reduces Ad5-induced lyso/LE dispersal, in contrast to LIC1 wild-type rescue cells. Ad5 capsid redistribution at 30 min p.i. shows similar virus burden in both cells. Lines depict cell outlines. (E) Quantification of data in D. Mean of three independent experiments with >40 cells each; error bars represent SDs. *, $P < 0.05$; **, $P < 0.01$. Bars, 20 µm.

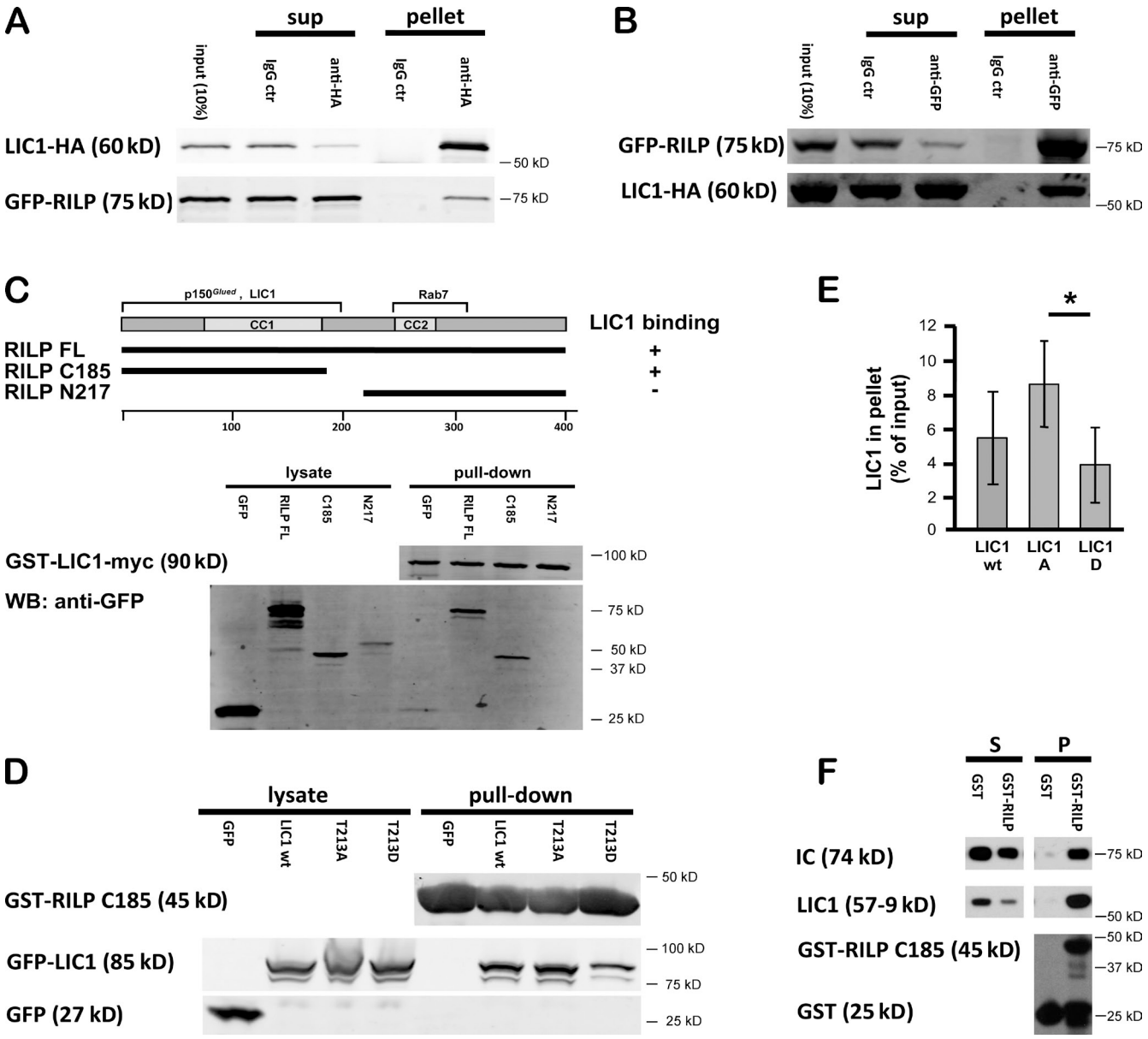

Figure 6. **Interaction of dynein with RILP.** (A) LIC1-HA was coexpressed with GFP-RILP and tested for coimmunoprecipitation with an anti-HA mAb. GFP-RILP coimmunoprecipitated with LIC1. ctr, control; sup, supernatant. (B) Reciprocal experiment showing LIC1-HA coimmunoprecipitation with GFP-RILP using an anti-GFP antibody. (C) Mapping of LIC1 interaction site in RILP by GST-LIC1 pull-down of 293A cell-expressed GFP-RILP full-length (FL), 1–185, and 217–401 (C33). Diagram shows RILP constructs and summarizes binding regions for Rab7, dynactin, and dynein. WB, Western blot. (D) GST-RILP 1–185 pull-down experiments using a 293A cell lysate expressing GFP or LIC1 wild type (wt), LIC1-T213A, and LIC1-T213D. Lysate and pellet samples were evaluated for pull-down of LIC1 by immunoblotting with antibodies against GFP. (E) Quantification of data in D. Mean of three independent experiments; error bars represent SDs. RILP 1–185 pulls down more LIC1-T213A than LIC1 wild type or LIC1-T213D. *, $P < 0.05$. (F) GST-RILP 1–185 pull-down experiments using purified rat brain dynein. Supernatant (S) and pellet (P) samples were evaluated for pull-down of the dynein complex by immunoblotting with antibodies against IC, LIC1, and GST.

mechanism to reach the nucleus quickly, avoiding intracellular innate immunity responses and degradation (Mallery et al., 2010). How widespread this scenario may be among viruses in general remains to be explored.

Our identification of a LIC1-mediated dynein regulatory mechanism may also have further, more general physiological implications. PKA activates dispersal of pigment granules in vertebrate chromatophores (Reilein et al., 1998; Marks and Seabra, 2001), but the targets of PKA phosphorylation are unknown. LIC1 now emerges as a candidate for this function. We also note that the site of PKA phosphorylation in LIC1, T213, is near S207 (S197 in *Xenopus laevis* LIC1), a Cdk1 site correlated with dynein dissociation from membranes during mitosis (Niclas et al., 1996; Dell et al., 2000; Addinall et al., 2001). Further analysis of these phenomena should shed important light not only on innate responses to virus infection but also cell cycle–dependent, stress-mediated (Korolchuk et al., 2011), and other aspects of lyso/LE distribution.

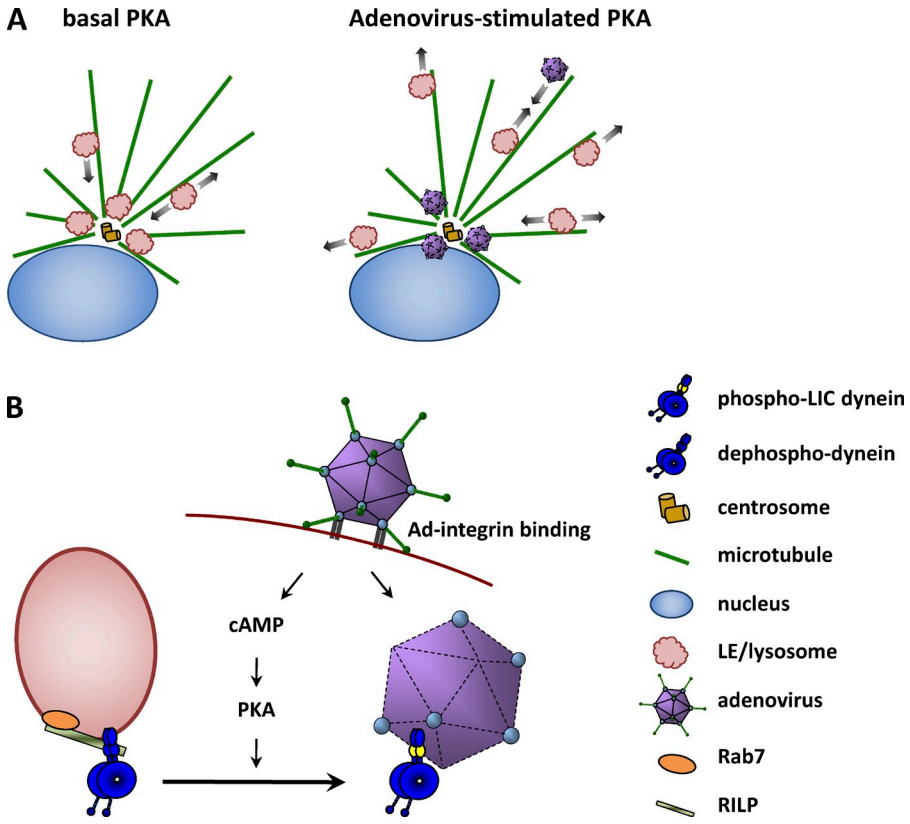

Figure 7. **Schematic representation of adenovirus-induced effects on dynein-mediated lyso/LE distribution and mechanism of PKA-mediated effects.** (A) At basal PKA activity levels in uninfected cells, lyso/LE cluster around the centrosome. At the onset of infection, adenovirus binds integrins, increasing cAMP levels and PKA activity. PKA phosphorylation of the dynein LIC1 subunit promotes virus transport to the centrosome and nucleus, while dispersing lyso/LEs in a novel mechanism for host–virus competition. (B) Dephosphorylated LIC1 mediates dynein recruitment to the lyso/LEs surface protein RILP, which is, in turn, recruited by activated Rab7. Upon infection, adenovirus–integrin binding leads to cAMP synthesis and PKA activation. LIC1 phosphorylation results in dynein switching from RILP to the virus capsid subunit hexon. Additional factors proposed to contribute to dynein recruitment to lyso/LEs are not depicted here but are described in the Discussion.

Materials and methods

Cellular and molecular reagents

A549 and 293A cells were grown in DMEM supplemented with 10% FBS. Amplification, purification, and labeling of replication-deficient Ad5 was engineered for late GFP expression (H. Young, Columbia University, New York, NY) as previously described (Bremner et al., 2009). Handling of wild-type Ad3 (VR-3; ATCC) and conjugation with Alexa Fluor 546 was as previously described for Ad5 (Bremner et al., 2009). Antibodies used included mouse monoclonal anti-hexon (Novocastra/Leica), anti-HA (clone 16B12; Covance), anti-FLAG (M2; Sigma-Aldrich), anti-myc (9E10; Santa Cruz Biotechnology, Inc.), anti-tubulin (Sigma-Aldrich), anti-p150^{Glued} (BD), anti–dynein IC (74.1; EMD Millipore), rabbit antibodies anti-LIC (Tynan et al., 2000a), anti-LIC2 (Tynan et al., 2000a), anti-Ad5 (Abcam), anti-Arp1 (Sigma-Aldrich), anti–dynein heavy chain (Mikami et al., 1993), anti-Lamp1 (Abcam), anti-GFP (Invitrogen), anti-FLAG (Abcam), anti-HA (Sigma-Aldrich), rabbit antibodies recognizing the phosphorylated PKA substrate motif RRXp(S/T) or RXXp(S/T) obtained from Cell Signaling Technology, and chicken anti-LIC1 (Tan et al., 2011) and anti-GFP (EMD Millipore). LysoTracker and MitoTracker green (Invitrogen) were used to label lysosomes and mitochondria, respectively. Mammalian expression constructs used in this work included LIC1 truncations C173, N174, C348, and N349 (all obtained from Tynan et al., 2000b) and full-length GFP-tagged versions of Rab7, RILP (both obtained from Tan et al., 2011), NPC1, Lamp1, Rab5, and NAGT (all obtained from Yi et al., 2011). Rat LIC1 was subcloned into the pEGFP-C1 vector (Takara Bio Inc.) by introducing 5′ XhoI and 3′ KpnI restriction sites by PCR. Resistance to LIC1 RNAi was archived as previously described (Tan et al., 2011). LIC1 point mutants were generated by site-directed mutagenesis (QuikChange II; Agilent Technologies) using primer sequences 5′-CCCCTCAGCGAAGAGCC**G**CGGCTGCACAGG-3′ and 5′-CCCCTCAGCGAAGAGCC**GAT**GCTGCACAGG-3′ for T213A and T213D, respectively (mutations in bold letters). For RNAi, shRNA constructs based on the pRetro-U6G vector (Cellogenetics) were used; the sequence for pRETRO-LIC1 is 5′-GTTGATTAGAGACTTCCAATT-3′, for pRETRO-LIC2, it is 5′-GCCAGAAGATGCATATGAA-3′, and for the scrambled control, it is 5′-CTTCATTAGAGAGTTCCAA-3′. The RNA sequence used for LIC1 siRNA was 5′-GUUGAUUAGAGACUUCCAATT-3′, and for LIC2 siRNA, it was 5′-GGAUAGAAUGACUCGAAAAUU-3′ (Tan et al., 2011). Transient transfections were performed using either Lipofectamine 2000 (Invitrogen) or Effectene (QIAGEN). siRNA oligonucleotides were transfected with HiPerFect (QIAGEN). Cloning of bacterial expression constructs of His-tagged full-length LIC1 and LIC2 constructs was described previously (Tynan et al., 2000b) and subjected to the aforementioned mutagenesis. GST-tagged full-length LIC1 was cloned into the pGEX-6p vector (GE Healthcare) using EcoRI–XhoI sites and C-terminal myc, and His tags were introduced by PCR. GST-tagged LC8 was described previously (McKenney et al., 2011), and full-length rat IC1A and IC2C were cloned in frame with GST into the pGEX-6p vector using BamHI–XhoI and BamHI–EcoRI sites, respectively. An additional C-terminal His tag was introduced by PCR. RILP-C185 was cloned into the pEGFP-C1 or pGEX-6p vectors by introducing EcoRI–BamHI or BamH1–EcoR1 restriction sites by PCR, respectively.

Virus infection and other cellular methods

A549 cells were typically infected with Ad5-GFP (Bremner et al., 2009) at an MOI of 20 in a low volume of DMEM lacking FBS at 4°C for 30 min to allow virus attachment. The cells were washed twice in cold PBS and incubated in fresh, warm DMEM/10% FBS for 60 min at 37°C to allow internalization and intracellular transport. For tests of adenovirus infectivity, an adaptation of the standard assay was used. A549 cells were infected as described above (typical infection) except at an MOI of 1 and were kept at 37°C for 24 h thereafter. Importantly, purified Ad5-GFP capsids were prelabeled with mouse monoclonal anti-hexon antibody for 30 min at 4°C at a 240:1 antibody/capsid ratio before inoculation. As in the standard assay, mean GFP fluorescence of the infected cell population was used as an infectivity marker. For fixed imaging, cells were grown on glass coverslips and exposed to methanol at −20°C for 5 min or with 4% PFA/PBS at RT for 15 min. Coverslips were blocked for >60 min in 0.5% donkey serum/PBS, incubated in primary antibody at 37°C for 1 h, washed, and incubated for 1 h at 37°C in Cy2-, Cy3-, or Cy5-conjugated secondary antibody. Then, they were mounted using antifade mounting media containing DAPI (ProLong gold; Invitrogen) and imaged using a confocal microscope (IX-81 with FV100 spectral confocal system; Olympus) equipped with 63×, 1.42 NA and 100×, 1.40 NA oil immersion objectives and operated with FluoView imaging software (Olympus). To evaluate infectivity, mean GFP fluorescence was compared per field of view using a 10×, 0.40 NA air

objective. For evaluation of virus redistribution, virus particles were scored as reaching the nucleus if they were <1 µm from the nuclear surface. To quantify changes in lyso/LE distribution, the maximum distance from the nuclear center to the cell margin was determined, and lyso/LEs were scored for their presence within 1/3, 2/3, and 3/3 of this distance (see also Fig. 5 B). For live imaging, cells were grown in glass-bottomed dishes (MatTek Corporation) and infected with unlabeled adenovirus at 100 MOI at 37°C for 5 min to synchronize virus attachment and entry and avoid low temperature–induced MT disassembly. The cells were transferred to CO_2-independent medium (Invitrogen) and then imaged in a 37°C chamber. Videos were typically acquired for 90 min p.i. at two frames/min using a 63×, 1.32 NA oil immersion objective and a charge-coupled device camera (model C9100-12; Hamamatsu Photonics) mounted on an inverted microscope (DM IRBE; Leica) operated by MetaMorph imaging software (Molecular Devices). All videos and images were analyzed using ImageJ (National Institutes of Health). For particle tracking, videos of Alexa Fluor 546–labeled Ad5 capsids were acquired 15–45 min p.i. at 37°C in CO_2-independent medium (Invitrogen) with the same microscope setup but at a 16.7-Hz frame rate for 30 s using a 100×, 1.40 NA oil immersion objective (actual pixel size of ∼160 nm/pixel). For motility analysis, a custom-tracking algorithm was used to extract the position of motile particles as previously described (Bremner et al., 2009). In brief, positions of each particle were obtained from Gaussian fit of the particle's fluorescent intensity. A motile particle was defined as any particle moving above the diffusive rate (Bremner et al., 2009). We tracked all particles persisting for ≥50 frames (3 s; Fig. S2). When indicated, cells were exposed 60 min before infection to the PKA inhibitors H-89 (Sigma-Aldrich) or PKI-myr (Enzo Life Sciences), the adenylyl cyclase activator forskolin (Sigma-Aldrich), the integrin inhibitor cyclic RGD (Enzo Life Sciences), and the phosphodiesterase inhibitor 3-isobutyl-1-methylxanthine (Santa Cruz Biotechnology, Inc.).

Proteins and biochemical analysis

Rat brain lysate and purified rat cytoplasmic dynein were prepared in phosphate-glutamate buffer, pH 7.0, as previously described (Paschal et al., 1987). In brief, MTs in rat brain lysate were assembled with the aid of 30 µM taxol (Sigma-Aldrich) and collected by centrifugation. Cytoplasmic dynein was released from MTs with 10 mM ATP (Sigma-Aldrich) and further purified on a linear sucrose gradient. The dynein fraction was essentially free of dynactin as assayed by immunoblotting (McKenney et al., 2010). Vectors for GST- and His-tagged dynein subunits were transformed into BL21-Gold(DE3)pLysS *Escherichia coli* (Agilent Technologies) and expressed for 3–5 h at 17 or 20°C after 15-min ice shock of Luria broth cultures at OD_{600} = 0.6 and induction with 0.5 mM IPTG. Purification was performed following standard procedures involving application to Ni^+–nitrilotriacetic acid (Sigma-Aldrich) in 30 mM TrisHCl, 150 mM NaCl, 5 mM imidazole, and 5 mM β-mercaptoethanol, pH 7.4, supplemented with a protease inhibitor cocktail (Sigma-Aldrich), and eluted with the same buffer containing 450 mM NaCl and 200 mM imidazole. GST-tagged polypeptides were applied to glutathione (USB/Affymetrix) beads in 10 mM TrisHCl, 150 mM NaCl, 1 mM EDTA, and 0.5 mM DTT, pH 7.4, supplemented with protease inhibitor cocktail, and eluted with 10 mM of reduced glutathione or cleaved from the GST using R3C protease. λ-PPase was purchased from New England Biolabs, Inc., purified PKA catalytic subunit was obtained from Sigma-Aldrich, and each was used according to instructions. For serial PPase/PKA treatments, PPase was inactivated with PPase inhibitors (50 mM NaF, 5 mM tetra-sodium pyrophosphate, 1 mM sodium orthovanadate, and 10 mM β-glyceropyrophosphate) before subsequent PKA treatment. Hexon binding assays were described previously (Bremner et al., 2009). In brief, hexon was immunoprecipitated from the soluble fraction of late-stage adenovirus-infected 293A cells using a hexon-specific monoclonal antibody linked to protein A–Sepharose beads (GE Healthcare). Beads were transferred into 50 mM Trizma-maleate, 10 mM NaCl, 1 mM EDTA, and 0.1% Tween 20, at pH 4.4, for 30 min and then into the same buffer at pH 7.4. The immunoisolated hexon was subsequently exposed to purified cytoplasmic dynein or bacterially expressed dynein subunits at 4°C for 1.5 h and washed, and the bound fraction was analyzed by immunoblotting. For LIC1 interaction experiments with RILP, GFP- or HA-tagged LIC1 constructs were coexpressed with GFP-tagged RILP constructs for 24 h in 293A cells, or GST-tagged proteins were used for pull-downs from lysates of RILP- or LIC1-overexpressing cells. Full-length and C33 RILP constructs were a gift from C. Bucci (University of Lecce, Lecce, Italy). Cells were lysed with radioimmunoprecipitation assay buffer (10 mM TrisHCl, 150 mM NaCl, 1 mM EDTA, and 1 mM EGTA, pH 7.4) and 0.5% NP-40, and the lysate was incubated for coimmunoprecipitations with monoclonal anti-HA or polyclonal anti-GFP antibodies linked to Sepharose A beads or for pull-downs with GST-tagged protein bound to glutathione beads at 4°C for 1.5 h and washed, and the unbound (supernatant) and bound (pellet) fractions were analyzed by immunoblotting. Immunoblots were incubated with fluorescently tagged secondary antibodies (Rockland Immunochemicals) and developed at subsaturating conditions using a scanning device (Odyssey; LI-COR Biosciences) and Odyssey software version 3.0, which allows us to maintain a linear relationship between signal and protein amount.

Statistical analysis

For analysis, two-sample comparisons were performed via Student's *t* test. Statistical significance was inferred for $P < 0.05$. Analysis and statistical tests were performed using Excel (Microsoft) and Prism (GraphPad Software).

Online supplemental material

Fig. S1 shows biochemical analysis of the dynein interactions with hexon and RILP. Fig. S2 and S3 show particle tracking of Ad5 capsids in A549 cells transfected with control or LIC1 shRNA constructs or LIC1 siRNA and rescue constructs, respectively. Fig. S4 shows lysosome dispersal induced by Ad5 infection. Fig. S5 shows LysoTracker red colocalization with vesicular markers. Video 1 shows Alexa Fluor 546–Ad5 motility in untreated cells. Video 2 shows Alexa Fluor 546–Ad5 motility in control siRNA-treated cells. Video 3 shows Alexa Fluor 546–Ad5 motility in LIC1 siRNA-treated cells. Video 4 shows Alexa Fluor 546–Ad5 motility in LIC1 wild-type rescue cells. Video 5 shows Alexa Fluor 546–Ad5 motility in LIC1-T213D rescue cells. Video 6 shows Alexa Fluor 546–Ad5 motility in LIC1-T213A rescue cells. Video 7 shows lysosome motility in an uninfected A549 cell. Video 8 shows lysosome motility in Ad5-infected A549 cells. Video 9 shows lysosome motility in Ad5-infected A549 cells treated with PKA inhibitor. Video 10 shows additional examples of lysosome motility in Ad5-infected A549 cells. Table S1 shows a summary of statistical parameters of live cell imaging data. Online supplemental material is available at http://www.jcb.org/cgi/content/full/jcb.201307116/DC1.

We thank Dr. Sarah Weil for comments on the manuscript, the dynein LC protein, and the GST-IC2 plasmid, Dr. Pascale Monzo for the GFP-LIC plasmids, and Dr. Kevin Vaughan, Dr. Vincent Racaniello, Dr. Yinghui Mao, Dr. Chloe Bulinski, and Dr. Gilbert Di Paolo as well as members of the Vallee laboratory for critical discussions.

This work was supported by National Institutes of Health grant GM102347.

The authors declare no competing financial interests.

Submitted: 22 July 2013
Accepted: 18 March 2014

References

Addinall, S.G., P.S. Mayr, S. Doyle, J.K. Sheehan, P.G. Woodman, and V.J. Allan. 2001. Phosphorylation by cdc2-CyclinB1 kinase releases cytoplasmic dynein from membranes. *J. Biol. Chem.* 276:15939–15944. http://dx.doi.org/10.1074/jbc.M011628200

Akhmanova, A., and J.A. Hammer III. 2010. Linking molecular motors to membrane cargo. *Curr. Opin. Cell Biol.* 22:479–487. http://dx.doi.org/10.1016/j.ceb.2010.04.008

Ally, S., A.G. Larson, K. Barlan, S.E. Rice, and V.I. Gelfand. 2009. Opposite-polarity motors activate one another to trigger cargo transport in live cells. *J. Cell Biol.* 187:1071–1082. http://dx.doi.org/10.1083/jcb.200908075

Andrews, N.W. 1995. Lysosome recruitment during host cell invasion by *Trypanosoma cruzi*. *Trends Cell Biol.* 5:133–137. http://dx.doi.org/10.1016/S0962-8924(00)88965-5

Barbar, E. 2012. Native disorder mediates binding of dynein to NudE and dynactin. *Biochem. Soc. Trans.* 40:1009–1013. http://dx.doi.org/10.1042/BST20120180

Bremner, K.H., J. Scherer, J. Yi, M. Vershinin, S.P. Gross, and R.B. Vallee. 2009. Adenovirus transport via direct interaction of cytoplasmic dynein with the viral capsid hexon subunit. *Cell Host Microbe*. 6:523–535. http://dx.doi.org/10.1016/j.chom.2009.11.006

Cantalupo, G., P. Alifano, V. Roberti, C.B. Bruni, and C. Bucci. 2001. Rab-interacting lysosomal protein (RILP): the Rab7 effector required for transport to lysosomes. *EMBO J.* 20:683–693. http://dx.doi.org/10.1093/emboj/20.4.683

Carette, J.E., M. Raaben, A.C. Wong, A.S. Herbert, G. Obernosterer, N. Mulherkar, A.I. Kuehne, P.J. Kranzusch, A.M. Griffin, G. Ruthel, et al. 2011. Ebola virus entry requires the cholesterol transporter Niemann-Pick C1. *Nature*. 477:340–343. http://dx.doi.org/10.1038/nature10348

Carey, B., M.K. Staudt, D. Bonaminio, J.C. van der Loo, and B.C. Trapnell. 2007. PU.1 redirects adenovirus to lysosomes in alveolar macrophages, uncoupling internalization from infection. *J. Immunol.* 178:2440–2447.

Caviston, J.P., and E.L. Holzbaur. 2006. Microtubule motors at the intersection of trafficking and transport. *Trends Cell Biol.* 16:530–537. http://dx.doi.org/10.1016/j.tcb.2006.08.002

Caviston, J.P., A.L. Zajac, M. Tokito, and E.L. Holzbaur. 2011. Huntingtin coordinates the dynein-mediated dynamic positioning of endosomes and lysosomes. *Mol. Biol. Cell*. 22:478–492. http://dx.doi.org/10.1091/mbc.E10-03-0233

Chardonnet, Y., and S. Dales. 1970. Early events in the interaction of adenoviruses with HeLa cells. I. Penetration of type 5 and intracellular release of the DNA genome. *Virology*. 40:462–477. http://dx.doi.org/10.1016/0042-6822(70)90189-3

Côté, M., J. Misasi, T. Ren, A. Bruchez, K. Lee, C.M. Filone, L. Hensley, Q. Li, D. Ory, K. Chandran, and J. Cunningham. 2011. Small molecule inhibitors reveal Niemann-Pick C1 is essential for Ebola virus infection. *Nature*. 477:344–348. http://dx.doi.org/10.1038/nature10380

Dell, K.R., C.W. Turck, and R.D. Vale. 2000. Mitotic phosphorylation of the dynein light intermediate chain is mediated by cdc2 kinase. *Traffic*. 1:38–44. http://dx.doi.org/10.1034/j.1600-0854.2000.010107.x

Dodding, M.P., and M. Way. 2011. Coupling viruses to dynein and kinesin-1. *EMBO J.* 30:3527–3539. http://dx.doi.org/10.1038/emboj.2011.283

Engelke, M.F., C.J. Burckhardt, M.K. Morf, and U.F. Greber. 2011. The dynactin complex enhances the speed of microtubule-dependent motions of adenovirus both towards and away from the nucleus. *Viruses*. 3:233–253. http://dx.doi.org/10.3390/v3030233

Enquist, L.W. 2012. Five questions about viral trafficking in neurons. *PLoS Pathog.* 8:e1002472. http://dx.doi.org/10.1371/journal.ppat.1002472

Greber, U.F., and M. Way. 2006. A superhighway to virus infection. *Cell*. 124:741–754. http://dx.doi.org/10.1016/j.cell.2006.02.018

Greber, U.F., M. Willetts, P. Webster, and A. Helenius. 1993. Stepwise dismantling of adenovirus 2 during entry into cells. *Cell*. 75:477–486. http://dx.doi.org/10.1016/0092-8674(93)90382-Z

Herman, B., and D.F. Albertini. 1983. Ligand-induced rapid redistribution of lysosomes is temporally distinct from endosome translocation. *Nature*. 304:738–740. http://dx.doi.org/10.1038/304738a0

Holleran, E.A., M.K. Tokito, S. Karki, and E.L. Holzbaur. 1996. Centractin (ARP1) associates with spectrin revealing a potential mechanism to link dynactin to intracellular organelles. *J. Cell Biol.* 135:1815–1829. http://dx.doi.org/10.1083/jcb.135.6.1815

Horgan, C.P., S.R. Hanscom, R.S. Jolly, C.E. Futter, and M.W. McCaffrey. 2010. Rab11-FIP3 links the Rab11 GTPase and cytoplasmic dynein to mediate transport to the endosomal-recycling compartment. *J. Cell Sci.* 123:181–191. http://dx.doi.org/10.1242/jcs.052670

Hunt, S.D., A.K. Townley, C.M. Danson, P.J. Cullen, and D.J. Stephens. 2013. Microtubule motors mediate endosomal sorting by maintaining functional domain organization. *J. Cell Sci.* 126:2493–2501. http://dx.doi.org/10.1242/jcs.122317

Jordens, I., M. Fernandez-Borja, M. Marsman, S. Dusseljee, L. Janssen, J. Calafat, H. Janssen, R. Wubbolts, and J. Neefjes. 2001. The Rab7 effector protein RILP controls lysosomal transport by inducing the recruitment of dynein-dynactin motors. *Curr. Biol.* 11:1680–1685. http://dx.doi.org/10.1016/S0960-9822(01)00531-0

Kardon, J.R., and R.D. Vale. 2009. Regulators of the cytoplasmic dynein motor. *Nat. Rev. Mol. Cell Biol.* 10:854–865. http://dx.doi.org/10.1038/nrm2804

Kim, H., S.C. Ling, G.C. Rogers, C. Kural, P.R. Selvin, S.L. Rogers, and V.I. Gelfand. 2007. Microtubule binding by dynactin is required for microtubule organization but not cargo transport. *J. Cell Biol.* 176:641–651. http://dx.doi.org/10.1083/jcb.200608128

King, S.J., and T.A. Schroer. 2000. Dynactin increases the processivity of the cytoplasmic dynein motor. *Nat. Cell Biol.* 2:20–24. http://dx.doi.org/10.1038/71338

Korolchuk, V.I., S. Saiki, M. Lichtenberg, F.H. Siddiqi, E.A. Roberts, S. Imarisio, L. Jahreiss, S. Sarkar, M. Futter, F.M. Menzies, et al. 2011. Lysosomal positioning coordinates cellular nutrient responses. *Nat. Cell Biol.* 13:453–460. http://dx.doi.org/10.1038/ncb2204

Kramer, T., and L.W. Enquist. 2012. Alphaherpesvirus infection disrupts mitochondrial transport in neurons. *Cell Host Microbe*. 11:504–514. http://dx.doi.org/10.1016/j.chom.2012.03.005

Leopold, P.L., G. Kreitzer, N. Miyazawa, S. Rempel, K.K. Pfister, E. Rodriguez-Boulan, and R.G. Crystal. 2000. Dynein- and microtubule-mediated translocation of adenovirus serotype 5 occurs after endosomal lysis. *Hum. Gene Ther.* 11:151–165. http://dx.doi.org/10.1089/10430340050016238

Mallery, D.L., W.A. McEwan, S.R. Bidgood, G.J. Towers, C.M. Johnson, and L.C. James. 2010. Antibodies mediate intracellular immunity through tripartite motif-containing 21 (TRIM21). *Proc. Natl. Acad. Sci. USA*. 107:19985–19990. http://dx.doi.org/10.1073/pnas.1014074107

Marks, M.S., and M.C. Seabra. 2001. The melanosome: membrane dynamics in black and white. *Nat. Rev. Mol. Cell Biol.* 2:738–748. http://dx.doi.org/10.1038/35096009

Matanis, T., A. Akhmanova, P. Wulf, E. Del Nery, T. Weide, T. Stepanova, N. Galjart, F. Grosveld, B. Goud, C.I. De Zeeuw, et al. 2002. Bicaudal-D regulates COPI-independent Golgi-ER transport by recruiting the dynein-dynactin motor complex. *Nat. Cell Biol.* 4:986–992. http://dx.doi.org/10.1038/ncb891

McEwan, W.A., J.C. Tam, R.E. Watkinson, S.R. Bidgood, D.L. Mallery, and L.C. James. 2013. Intracellular antibody-bound pathogens stimulate immune signaling via the Fc receptor TRIM21. *Nat. Immunol.* 14:327–336. http://dx.doi.org/10.1038/ni.2548

McKenney, R.J., M. Vershinin, A. Kunwar, R.B. Vallee, and S.P. Gross. 2010. LIS1 and NudE induce a persistent dynein force-producing state. *Cell*. 141:304–314. http://dx.doi.org/10.1016/j.cell.2010.02.035

McKenney, R.J., S.J. Weil, J. Scherer, and R.B. Vallee. 2011. Mutually exclusive cytoplasmic dynein regulation by NudE-Lis1 and dynactin. *J. Biol. Chem.* 286:39615–39622. http://dx.doi.org/10.1074/jbc.M111.289017

Mikami, A., B.M. Paschal, M. Mazumdar, and R.B. Vallee. 1993. Molecular cloning of the retrograde transport motor cytoplasmic dynein (MAP 1C). *Neuron*. 10:787–796. http://dx.doi.org/10.1016/0896-6273(93)90195-W

Miyazawa, N., R.G. Crystal, and P.L. Leopold. 2001. Adenovirus serotype 7 retention in a late endosomal compartment prior to cytosol escape is modulated by fiber protein. *J. Virol.* 75:1387–1400. http://dx.doi.org/10.1128/JVI.75.3.1387-1400.2001

Niclas, J., V.J. Allan, and R.D. Vale. 1996. Cell cycle regulation of dynein association with membranes modulates microtubule-based organelle transport. *J. Cell Biol.* 133:585–593. http://dx.doi.org/10.1083/jcb.133.3.585

Palmer, K.J., H. Hughes, and D.J. Stephens. 2009. Specificity of cytoplasmic dynein subunits in discrete membrane-trafficking steps. *Mol. Biol. Cell*. 20:2885–2899. http://dx.doi.org/10.1091/mbc.E08-12-1160

Paschal, B.M., H.S. Shpetner, and R.B. Vallee. 1987. MAP 1C is a microtubule-activated ATPase which translocates microtubules in vitro and has dynein-like properties. *J. Cell Biol.* 105:1273–1282. http://dx.doi.org/10.1083/jcb.105.3.1273

Progida, C., L. Malerød, S. Stuffers, A. Brech, C. Bucci, and H. Stenmark. 2007. RILP is required for the proper morphology and function of late endosomes. *J. Cell Sci.* 120:3729–3737. http://dx.doi.org/10.1242/jcs.017301

Radtke, K., K. Döhner, and B. Sodeik. 2006. Viral interactions with the cytoskeleton: a hitchhiker's guide to the cell. *Cell. Microbiol.* 8:387–400. http://dx.doi.org/10.1111/j.1462-5822.2005.00679.x

Reilein, A.R., I.S. Tint, N.I. Peunova, G.N. Enikolopov, and V.I. Gelfand. 1998. Regulation of organelle movement in melanophores by protein kinase A (PKA), protein kinase C (PKC), and protein phosphatase 2A (PP2A). *J. Cell Biol.* 142:803–813. http://dx.doi.org/10.1083/jcb.142.3.803

Rocha, N., C. Kuijl, R. van der Kant, L. Janssen, D. Houben, H. Janssen, W. Zwart, and J. Neefjes. 2009. Cholesterol sensor ORP1L contacts the ER protein VAP to control Rab7–RILP–p150^{Glued} and late endosome positioning. *J. Cell Biol.* 185:1209–1225. http://dx.doi.org/10.1083/jcb.200811005

Rodionov, V., J. Yi, A. Kashina, A. Oladipo, and S.P. Gross. 2003. Switching between microtubule- and actin-based transport systems in melanophores is controlled by cAMP levels. *Curr. Biol.* 13:1837–1847. http://dx.doi.org/10.1016/j.cub.2003.10.027

Scherer, J., and R.B. Vallee. 2011. Adenovirus recruits dynein by an evolutionary novel mechanism involving direct binding to pH-primed hexon. *Viruses*. 3:1417–1431. http://dx.doi.org/10.3390/v3081417

Soppina, V., A.K. Rai, A.J. Ramaiya, P. Barak, and R. Mallik. 2009. Tug-of-war between dissimilar teams of microtubule motors regulates transport and fission of endosomes. *Proc. Natl. Acad. Sci. USA*. 106:19381–19386. http://dx.doi.org/10.1073/pnas.0906524106

Splinter, D., D.S. Razafsky, M.A. Schlager, A. Serra-Marques, I. Grigoriev, J. Demmers, N. Keijzer, K. Jiang, I. Poser, A.A. Hyman, et al. 2012. BICD2, dynactin, and LIS1 cooperate in regulating dynein recruitment to cellular structures. *Mol. Biol. Cell*. 23:4226–4241. http://dx.doi.org/10.1091/mbc.E12-03-0210

Suomalainen, M., M.Y. Nakano, S. Keller, K. Boucke, R.P. Stidwill, and U.F. Greber. 1999. Microtubule-dependent plus- and minus end–directed motilities are competing processes for nuclear targeting of adenovirus. *J. Cell Biol.* 144:657–672. http://dx.doi.org/10.1083/jcb.144.4.657

Suomalainen, M., M.Y. Nakano, K. Boucke, S. Keller, and U.F. Greber. 2001. Adenovirus-activated PKA and p38/MAPK pathways boost microtubule-mediated nuclear targeting of virus. *EMBO J.* 20:1310–1319. http://dx.doi.org/10.1093/emboj/20.6.1310

Tan, S.C., J. Scherer, and R.B. Vallee. 2011. Recruitment of dynein to late endosomes and lysosomes through light intermediate chains. *Mol. Biol. Cell*. 22:467–477. http://dx.doi.org/10.1091/mbc.E10-02-0129

Tardieux, I., P. Webster, J. Ravesloot, W. Boron, J.A. Lunn, J.E. Heuser, and N.W. Andrews. 1992. Lysosome recruitment and fusion are early events required for trypanosome invasion of mammalian cells. *Cell*. 71:1117–1130. http://dx.doi.org/10.1016/S0092-8674(05)80061-3

Tynan, S.H., M.A. Gee, and R.B. Vallee. 2000a. Distinct but overlapping sites within the cytoplasmic dynein heavy chain for dimerization and for intermediate chain and light intermediate chain binding. *J. Biol. Chem.* 275: 32769–32774. http://dx.doi.org/10.1074/jbc.M001537200

Tynan, S.H., A. Purohit, S.J. Doxsey, and R.B. Vallee. 2000b. Light intermediate chain 1 defines a functional subfraction of cytoplasmic dynein which binds to pericentrin. *J. Biol. Chem.* 275:32763–32768. http://dx.doi.org/10.1074/jbc.M001536200

Vallee, R.B., R.J. McKenney, and K.M. Ori-McKenney. 2012. Multiple modes of cytoplasmic dynein regulation. *Nat. Cell Biol.* 14:224–230. http://dx.doi.org/10.1038/ncb2420

van der Kant, R., A. Fish, L. Janssen, H. Janssen, S. Krom, N. Ho, T. Brummelkamp, J. Carette, N. Rocha, and J. Neefjes. 2013. Late endosomal transport and tethering are coupled processes controlled by RILP and the cholesterol sensor ORP1L. *J. Cell Sci.* 126:3462–3474. http://dx.doi.org/10.1242/jcs.129270

Wickham, T.J., P. Mathias, D.A. Cheresh, and G.R. Nemerow. 1993. Integrins alpha v beta 3 and alpha v beta 5 promote adenovirus internalization but not virus attachment. *Cell*. 73:309–319. http://dx.doi.org/10.1016/0092-8674(93)90231-E

Yi, J.Y., K.M. Ori-McKenney, R.J. McKenney, M. Vershinin, S.P. Gross, and R.B. Vallee. 2011. High-resolution imaging reveals indirect coordination of opposite motors and a role for LIS1 in high-load axonal transport. *J. Cell Biol.* 195:193–201. http://dx.doi.org/10.1083/jcb.201104076